AIAA SciTech Forum
8-12 January 2024, Orlando, FL
AIAA SCITECH 2024 Forum

10.2514/6.2024-0412

Thermal Deformation of Ultrathin Composite Structures in a Vacuum Environment

John Pederson* and Sergio Pellegrino†
Graduate Aerospace Laboratories, California Institute of Technology, Pasadena, CA, 91125

Deployable space structures experience thermally induced deformations on-orbit due to solar radiant heating. Deflection and temperature profiles under radiant heating are simulated for a section of a prototype deployable strip structure and verified experimentally. The simulation is extended to model structures with extended lengths (1, 2, and 5 m) under sunlight conditions. Results are compared with those of a small-scale experiment. The resulting deflection and temperature fields yield insight into the factors dominating the behavior of thin composite strip structures, specifically in-plane conductivity and axial twisting.

I. Introduction

Fitting within current rocket fairings requires large lightweight spacecraft structures to coil, bend, or otherwise fold into a smaller envelope for subsequent deployment on orbit. This combination of factors requires lightweight coilable structural elements that are stiff in bending when deployed; examples include the tape spring and the Triangular Rollable and Collapsible (TRAC) boom geometries [1]. However, in the vacuum of space, under radiant heat from the sun, thin lightweight booms experience rapid temperature changes and gradients; thermal expansion and contraction within the structure can then cause significant deformations [2]. These deflections tend to inhibit shape accuracy, disturb spacecraft pointing, and contribute to material fatigue – all of which have afflicted many space missions over the last sixty years [3].

The deflection response of steel tape springs under such radiant heating was previously investigated [4]. An experiment revealed the existence of surprisingly rich transient deflection behavior, while an accompanying multiphysics simulation was able to capture the same effects. While predicting the behavior of a single isolated tape spring illuminated by an infrared light may seem a far cry from predicting how a full deployable structure will react to sunlight, the tools and techniques used in our former study apply just as well to the latter. Measuring in- and out-of-plane deflection and temperature has allowed for the collection of real data on such parameters, and comparing this data with simulated data rendered subsequent simulations (both at the same scale and at a larger scale) able to be better trusted.

A compilation of analyses regarding thermal effects in space structures can be found in Earl Thornton's *Thermal Structures for Aerospace Applications* [3], along with overviews of the literature related to thermal control in airplanes and spacecraft and analytical and finite-element solutions to representative problems. The first step to analyzing thermal deformation of a boom – namely, the derivation of the steady-state temperature field under a radiant heat load – is provided and explained in Thornton's work. It provides a useful check on any preliminary simulation results, since solving for this field is the first step in any multiphysics simulation. Other works provide an insight into the deflection profiles of selected boom geometries, usually in the context of predicting thermal deflections of proposed or current spacecraft components. For example, Stohlman simulated steady-state deflections of TRAC booms, including those used on The Planetary Society's Lightsail-A, with some analysis of the effects of a vapor-deposited coating and a simulated composite with low coefficient of thermal expansion [1]. Stohlman also investigated the deflection of a cylindrical boom geometry in an analysis that coupled the heat transfer finite-element software Thermal Desktop with the dynamic finite-element software Abaqus using MATLAB scripts, comparing the results to a previous analysis performed by Blandino [1, 5]. Chamberlain, Kiefer, and Banik also performed an analysis of cylindrical booms, analyzing the split-cylinder composite booms of the Roll-Out Solar Array to determine the deflection and vibration modes induced by sunlight exposure under orbital conditions [6]. All of these works reveal the existence of large thermal gradients across thin structural booms due to the effect of boom geometry on local radiative heating.

As far as analyzing thermal effects on panel-like structures, a detailed analysis was performed by Thornton of the deflection and bending modes of the Hubble Space Telescope's deployable blanket solar arrays [3]. Other work has

*Ph.D. Candidate, Graduate Aerospace Laboratories, 1200 E. California Blvd., Mail Code 250-45. pederson@caltech.edu
†Joyce and Kent Kresa Professor of Aerospace and Civil Engineering, Jet Propulsion Laboratory Senior Research Scientist; Co-Director, Space-Based Solar Power Project, Graduate Aerospace Laboratories, 1200 E. California Blvd., Mail Code 105-50. AIAA Fellow. sergiop@caltech.edu

looked at radiative heating effects on truss structures made of thin rods. Mahaney and Thornton revealed that the effect of the rods shadowing each other had a significant impact on the trusses' thermostructural response [7]. These two works show how changes in the structure's geometry (by deflection or residual shape inaccuracies from manufacturing) can change the local radiation environment in any given part of the structure, causing twisting and bending effects that cannot be ignored in sufficiently large structures.

The main issue with simulations of long spacecraft booms and structures (> 1 m) is a simple one: to the authors' best knowledge, none in the literature produce direct experimental evidence that matches the predictions of the simulation. In addition, despite predicting *larger* thermal gradients, many previous works have simulated composite structures to have *smaller* thermal deflections due to their theoretically lower coefficients of thermal expansion [1]. However, based on experimentally measured material properties and realistic material inhomogeneities (such as misaligned composite fibers), our simulations and experimental evidence demonstrate thermal deflections even *larger* than those of isotropic booms.

With such a discrepancy between previous simulations and current experiments, experimental verification of the predictions of our simulations – heating and measuring a small-scale unit of the structure in question – was both necessary and useful. The results of these tests were used to improve the multiphysics simulations, and after adjusting the heating and environment in the model, the results presented here were obtained.

In this work, a thin-shell deployable space structure is selected, and a representative unit of that structure is modeled in a multiphysics simulation software under sunlight-level radiant heating. The structural models are then extended to more realistic lengths (1 m, 2 m, and 5 m) and observed. Next, various parameters, – composite fiber misalignment, in-plane conductivitiy, and structural twist – are simulated to determine which have the greatest impact on structural temperature and deflection profiles. Attempts to simulate geometrically nonlinear deflections with the current software are presented, and the shortcomings of currently available simulation software identified. Finally, the results of small-scale simulation are corroborated with experimental results from radiatively heating a unit structure under near-vacuum and measuring its deflection and temperatures.

II. Sample Structure Selection and Properties

The structure to be examined is a section of a much larger structure known as the Deployable on-Orbit ultraLight Composite Experiment (DOLCE) – namely, a two-meter prototype of the structural architecture proposed for the Space Solar Power Project, as demonstrated on the SSPD-1 mission [8]. Designed to be coiled, stowed for launch, uncoiled, and dynamically deployed on orbit, this architecture uses trapezoidal "strips" composed of ultrathin composite shell longerons that can be folded in the manner of an accordion, then coiled around a central hub for stowage, as shown in Figure 1. These trapezoidal strips are comprised of two TRAC longerons connected by carbon-fiber battens; the spacing between the longerons is nominally 20 cm, while the batten spacing is variable to allow for varying strip length.

This work studies a sample strip formed of two 25 cm longerons and two battens, spaced 20 and 24 cm apart, respectively, for a total footprint of around 25 cm by 25 cm, as pictured in Figure 1. This is the basic unit of the strip architecture, one that still preserves the key areas of interest regarding thermal behavior – namely, full-size longerons and battens, realistic mechanical and thermal interfaces between the two, and unavoidable manufacturing defects – to gain a more representative understanding of how a larger structure might behave.

A. Unit Structural Properties

A key aspect of this sample strip, heavily influencing its thermal behavior and deflection, is its construction from ultrathin composite materials. While the battens are simply off-the-shelf pultruded carbon-fiber rods with a rectangular cross-section [9] [8], 25-gsm glass-fiber plain-weave prepreg and 30-gsm unidirectional carbon-fiber prepreg sheets were combined to manufacture the longerons; the curved flanges are a three-ply laminate [±45 GFPW / 0 UDCF/ ±45 GFPW], while the web connecting them is a seven-ply laminate [±45 GFPW / 0 UDCF / ±45 $GFPW_3$ / 0 UDCF / ±45 GFPW]. Effectively, the web is formed from the material of the two flanges bonded together lengthwise with an additional GFPW lamina in between. The structural properties of the constituent laminae are detailed in Table 1.

B. Unit Thermal Properties

While the mechanical properties of these laminae and laminates have been previously characterized [10], the required thermal properties (specific heat, density, coefficient of thermal expansion, and conductivity) had to be measured directly from tests performed on coupons of the flange laminate. Measuring the thermal properties of the complete laminate left

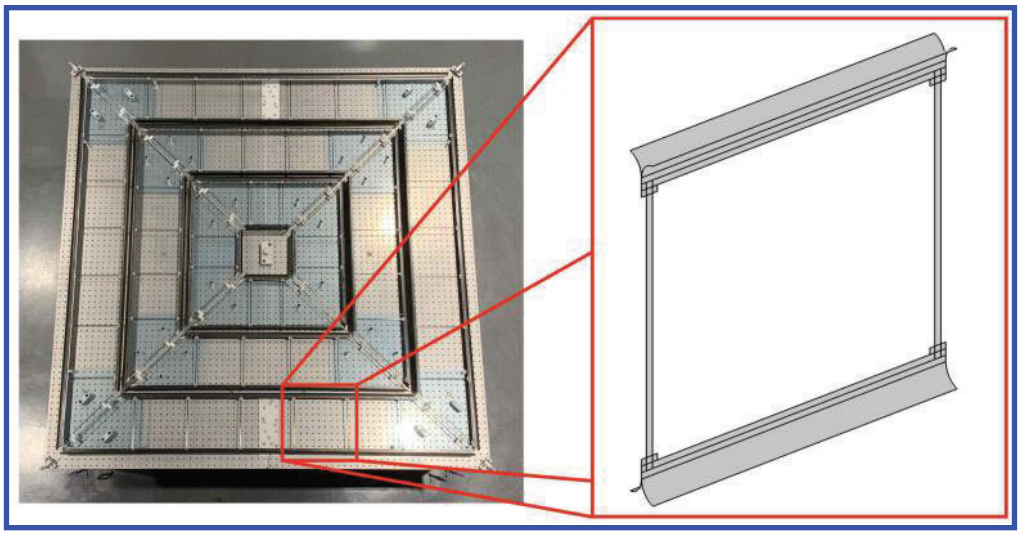

Fig. 1 The SSPD-1 structural framework, made of trapezoidal "strips" (left); the simulation model of the sample strip, a representative unit of the larger strip (right). The unit is approximately 25 cm by 25 cm.

the layers' individual thermal properties unknown, but was completely sufficient for thermal simulations of the full laminate. The thermal properties of the web laminate are given in Table 1.

The technique used to measure the thermal conductivity of the composite laminate will be detailed in an upcoming publication. To summarize the method, a 30 mW laser illuminated the center of a flat coupon of the laminate, and the resulting transient and steady-state temperature fields were measured with an infrared camera. A multiphysics simulation model of the test setup modeled this steady-state temperature field for many pairs of possible conductivities in the fiber direction and transverse direction of the laminate, taking into account the heating profile of the laser. The transient temperature data was used to inform which values of k_1 and k_2 were most likely to yield the experimental temperature field, narrowing the parameter space to be searched. The simulated results were then compared with experimental data via a MATLAB script, and the two in-plane conductivities that best matched experimental results were $k_1 = 0.99\frac{W}{m^2}$ and $k_2 = 0.27\frac{W}{m^2}$, with conservative bounds on the two values being $(0.66, 1.1]\frac{W}{m^2}$ and $(0, 0.66)\frac{W}{m^2}$, respectively. These values will be used as starting points for the analysis of in-plane thermal conductivity on temperature and deflection fields presented later.

Table 1 Laminae/laminate material properties. Structural properties are provided separately for each lamina, while thermal properties were determined via testing on the assembled laminate.

Glass-Fiber Plain-Weave		**Unidirectional Carbon Fiber**		**[±45 GFPW/0 UDCF/±45 GFPW] Laminate**	
E_1, E_2, E_3	128, 6.5, 6.5 GPa	E_1, E_2, E_3	128, 6.5, 6.5 GPa	k	$0.66\ \frac{W}{m\cdot K}$
$\nu_{12}, \nu_{13}, \nu_{23}$	0.35, 0.0178, 0.0178	$\nu_{12}, \nu_{13}, \nu_{23}$	0.35, 0.0178, 0.0178	$CTE_{12,13,23}$	$25.9, 19, 19 \times 10^{-6}\ \frac{1}{K}$
ρ	$1770\ \frac{kg}{m^3}$	ρ	$1770\ \frac{kg}{m^3}$	ϵ	0.89
t	$25\ \mu m$	t	$25\ \mu$m		
C_p	$461\ \frac{J}{kg\cdot K}$	C_p	$461\ \frac{J}{kg\cdot K}$		

III. Numerical Simulations in COMSOL Multiphysics

A series of simulations of the sample structure were then performed using the finite-element software COMSOL Multiphysics®, predicting the temperature fields and thermal deflections for the structures under radiant heating from one side.

In order to model the thermal-structural effects from radiant heating, as well as coupling among these effects, several

COMSOL modules were effectively chained together. Note that the entire strip geometry is constructed of thin shells – thus, only the shell elements, shell mechanics, and shell heat transfer modules of COMSOL were used. To model sunlight or infrared lamp light, the External Radiation Source of the Surface-to-Surface Radiation module was used; to model the transfer and spreading of heat among the shells of the strip, the Heat Transfer in Shells module was used, and was coupled to the Surface-to-Surface Radiation module by means of the Heat Transfer with Surface-to-Surface Radiation Multiphysics module. To model the thermal expansion of the shells, as well as to capture the clamped root boundary condition of the longeron, the Shell solid mechanics module was used, with a Thermal Expansion component added under the Layered Linear Elastic material definition.

The composite materials were modeled using the Layered Materials of the Composite Materials Module, the layers being the orthotropic glass-fiber plain-weave and unidirectional carbon-fiber laminates specified above. The mechanical properties of both laminae presented in Table 1 were used directly, while both laminae were given the same laminate thermal properties for the reasons explained in the previous section.

The radiation boundary condition in all cases models sunlight shining on the structure; parallel rays of light at a flux of 1361 $\frac{W}{m^2}$ are specified as an External Radiation Source. The initial temperatures, as well as the background radiation temperature, are set to 293.15 K, i.e. room temperature.

A. Single Strip Unit

The geometry of the basic unit was replicated in COMSOL using various geometries. The two longerons were formed from the union of three parametric surfaces: two cylindrical sections corresponding to the curved flanges, and one thicker rectangle joining them at one end corresponding to the web. The battens are rectangular prisms. In reality, the two longerons are joined to the battens using small rectangles of single-ply glass-fiber plain-weave composite; this attachment was modeled by means of the rectangles intersecting the battens and web, then forming a union of all three – see Figure 2. The separate components maintain their respective material properties, which were specified individually.

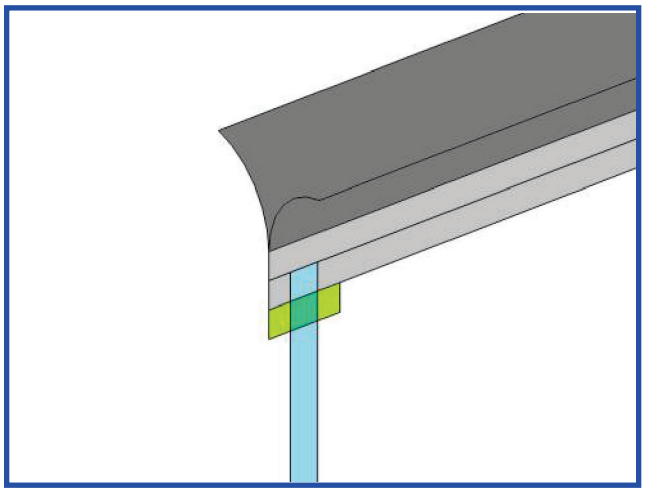

Fig. 2 A detail of the geometrical connection between the longeron web (light gray), batten (light blue), and glass-fiber plain-weave connecting tape (light green), with the overlap between the last two (green). The horizontal line splitting the web lengthwise is a non-physical internal boundary for better meshing.

1. Default Parameters

To start, we model the structure with nominal dimensions and no manufacturing defects; this ensures that the structure is symmetrically illuminated.

The results of running a stationary (i.e. steady-state) linear coupled analysis are shown in Figure 3, which shows temperature at left and y-deflection at right. Several things are immediately apparent – the first of which is the large thermally induced deflection effectively twisting the structure. The resulting y-deflection is over 13% of the structure's length in magnitude, meaning that an analysis of this structure assuming small deflections is likely to be inaccurate. While the thermal loads are *coupled* to the structural loads – i.e. the temperature field causes a thermal deflection field – the resulting *geometrical* nonlinearity must still be accounted for, which is done in Section III.D.

A detail of the temperature map, plotted on the undeformed structure for clarity, is shown in Figure 4 for a solar heat flux incident from the left. The effect of geometry and conduction on the temperature distribution is quite visible, and worth noting – the tip of the left flange, being parallel to the incoming heat flux, remains much cooler than the rest of the flange, only heating via conduction from the heated portion; in addition, the right flange remains much colder, only heating due to conduction through the web. The uniformity of the temperature field along the length of the longeron demonstrates the lack of accounting for large deflections.

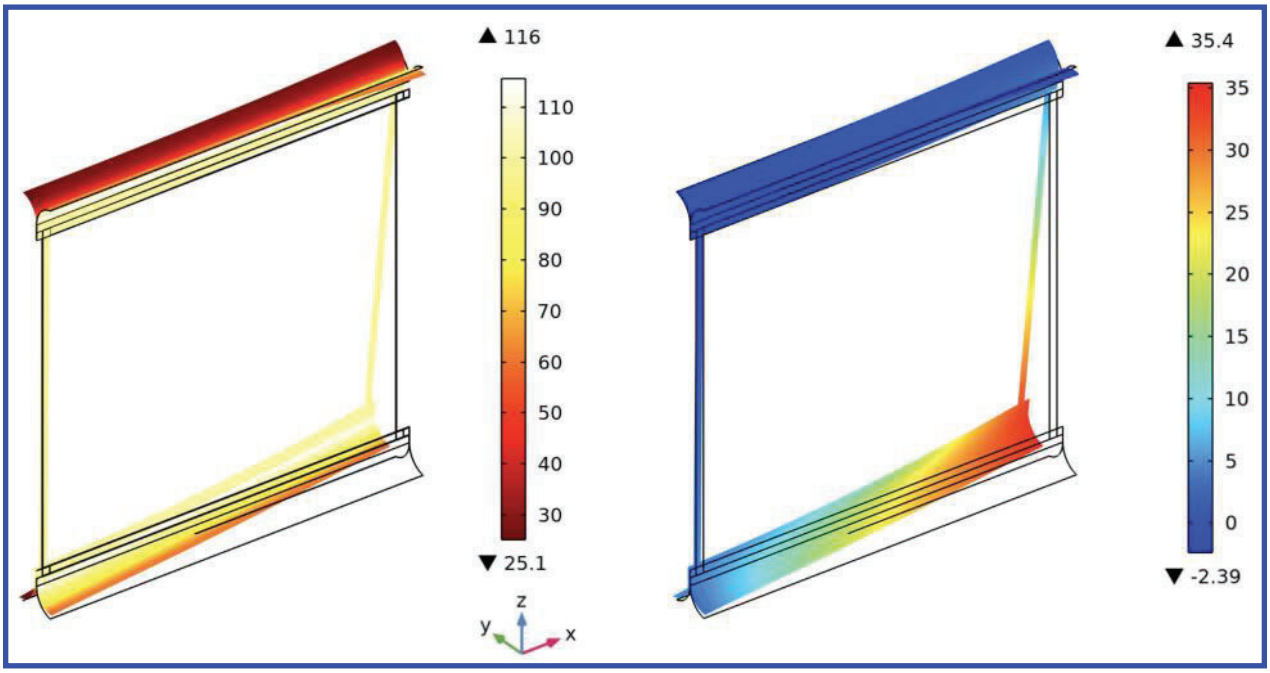

Fig. 3 Temperature (left, °C) and *y*-deflection (right, mm) results for the 25 cm strip unit. The structure is rigidly clamped at the upper left corner and free at all other points; solar heat flux shines on the sample in the +*y* direction. Black outline indicates the original unheated shape of the strip.

B. Structures with Multiple Units)

The strip geometry was then extended to lengths more representative of real space applications; the two longerons were extended to nominal lengths of 1 m, 2 m, and 5 m, with the number of battens correspondingly increased. In order to keep the same inter-batten distance of 241 mm, the longeron lengths were slightly adjusted to maintain an integer number of structural units and the same strip edge finishes; for example, the nominally 1 m strip is in fact 0.977 m long to be an exact multiple of four strip units. See Figure 5 for a more detailed view of the 1 m strip as an example.

1. Default Parameters

Stationary, coupled, geometrically linear simulations were run on all three lengths to obtain the *y*-displacement fields shown in Figure 6. The temperature fields of all three lengths are again uniform and lengthwise identical to the 25 cm model, due to the simulation not taking into account the large deflections and calculating the temperature field based on the undeflected structure. This fact means that such deflections may be of limited accuracy, but serve as a baseline case to compare the effects of in-plane conductivity, twisting, etc. without the confounding effect of nonlinear deformation affecting the heating and temperature profiles.

The length of the 5 m structure, however, renders it somewhat less useful for this baseline case, since a small change in deflection anywhere along the structure can affect the deflection field for the entire remaining length of the structure. While a local deflection change can affect the global deflection for several meters in the 5 m case, the same change can only affect the global deflection for tens of centimeters in the 1 m and 2 m case. Therefore, only the 25 cm, 1 m, and 2 m structures are shown for the remainder of these geometrically linear studies, with the 5 m structure only referenced as an extreme case.

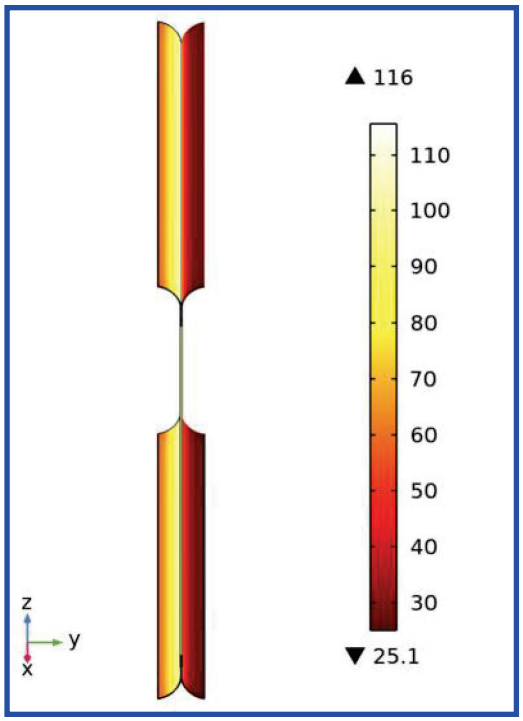

Fig. 4 Temperature (°C) map as plotted on the *undeformed* 25 cm structure depicted in Figure 3 at left. Solar heat flux is incident from the left. The effects of both geometry and conduction on surface temperature are present.

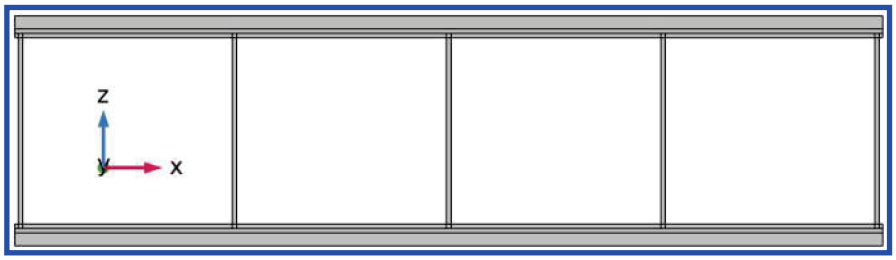

Fig. 5 Detail of the 1 m structure. The geometry preserves the distance between battens, fixed at .241 m, as well as the distance between the first and last batten and the longeron edges. Note that glass tapes connecting the battens to the main longeron are not modeled, as they do not have a significant effect on the structural deflection.

2. Effect of Fiber Misalignment

A common defect in composite laminates is fiber misalignment – namely, the orientation of the constituent fibers differing slightly from the nominal direction of a unidirectional lamina. Such defects can result in waviness of the fibers themselves as well as overall fiber misalignments (i.e. every fiber of the lamina parallel but pointing in a direction other than the nominal one) [11]. Due to the complexity of modeling the former, we will instead model the latter; we simply adjust the laminate model by rotating one of the constituent laminae a certain number of degrees, as shown in Figure 7. Fiber misalignment angles of up to 2° have been commonly observed experimentally [11], and this is the value used in this analysis. The modified laminate is then applied to both webs and two flanges, as shown in Figure 7 at left, and the same simulation performed again. This particular configuration of misaligned plies is the one that was found to result in the greatest amount of deflection difference.

The temperature field results, owing to the small-deflection assumption, are identical to the pristine laminate case; the deflection results are shown in Figure 7 at right and Figure 8 — only a small difference from the perfect laminate is detectable. Indeed, even at larger structural scales (2 m), the effect is negligible – Figure 8 shows a maximum of 2 mm greater deflection than the perfect laminate case, a difference of only 1.4%.

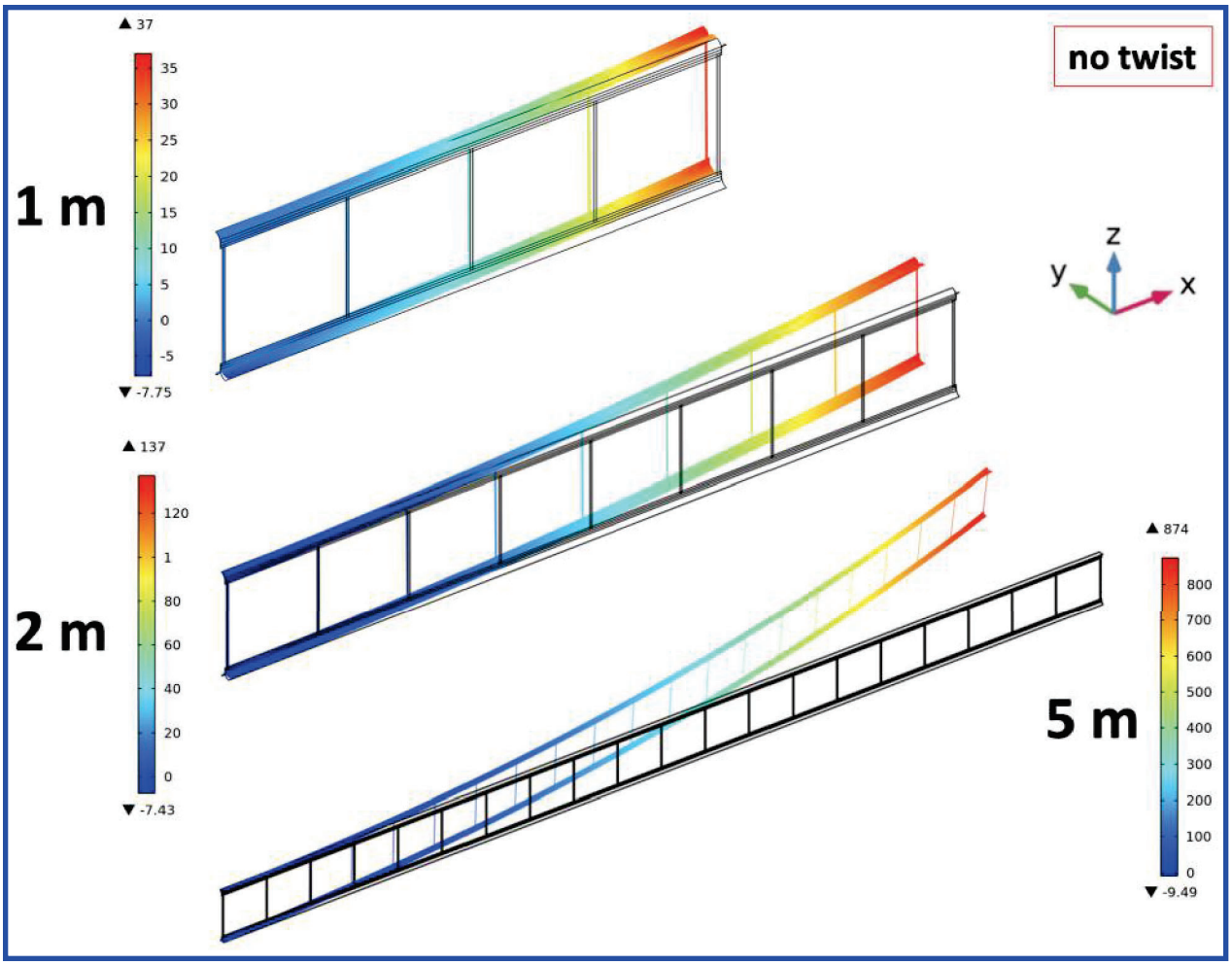

Fig. 6 Deflection (mm) profiles of the 1 m, 2 m, and 5 m strips clamped at the upper-right corner, without modeling geometric nonlinearity. The deflections are large compared to the structure, and the temperature field has not been recalculated for the deformed geometry; this deflection therefore serves as a base case.

C. Thermal Conduction at Root

The above simulations have a thermally insulated root boundary condition – i.e. no heat is allowed to flow into the root support of the structure. This may be an unrealistic assumption: a clamped boundary condition can only be achieved with direct physical contact, so a well-clamped boundary condition will also have good thermal contact. If the effect of root conduction is included, it may also offer a means of varying the temperature field along the structure, which would cause a corresponding variation of the thermal gradients leading to the final deflection field.

Since a clamp temperature that tracks the structure's root temperature would be identical to a thermally insulated clamp, fixing the clamp temperature at 20°C allows for heat to be conducted into the root.

1. Effect of k_1

The conductivity *along* the fiber direction, i.e. along the axis of the structure, might impact the steady-state temperatures and heat flow along the length of the structure when heat is allowed to flow into the root clamp. However, the simulation reveals that the nominal thermal conductivity of our laminates along the fiber direction ($\sim 0.99 \frac{W}{m^2 K}$) is small enough that the cooling effect of the root quickly dissipates within a few millimeters of the structure's end; see Figure 9 for a closer view of the heat-affected zone. As such, *the effect of heat conduction into the clamped root is negligible for our values of k_1*. Even values of k_1 two orders of magnitude higher, while penetrating a few centimeters into the longeron, still barely affect the global deflection of the structure; the maximum displacement of a 5 m structure

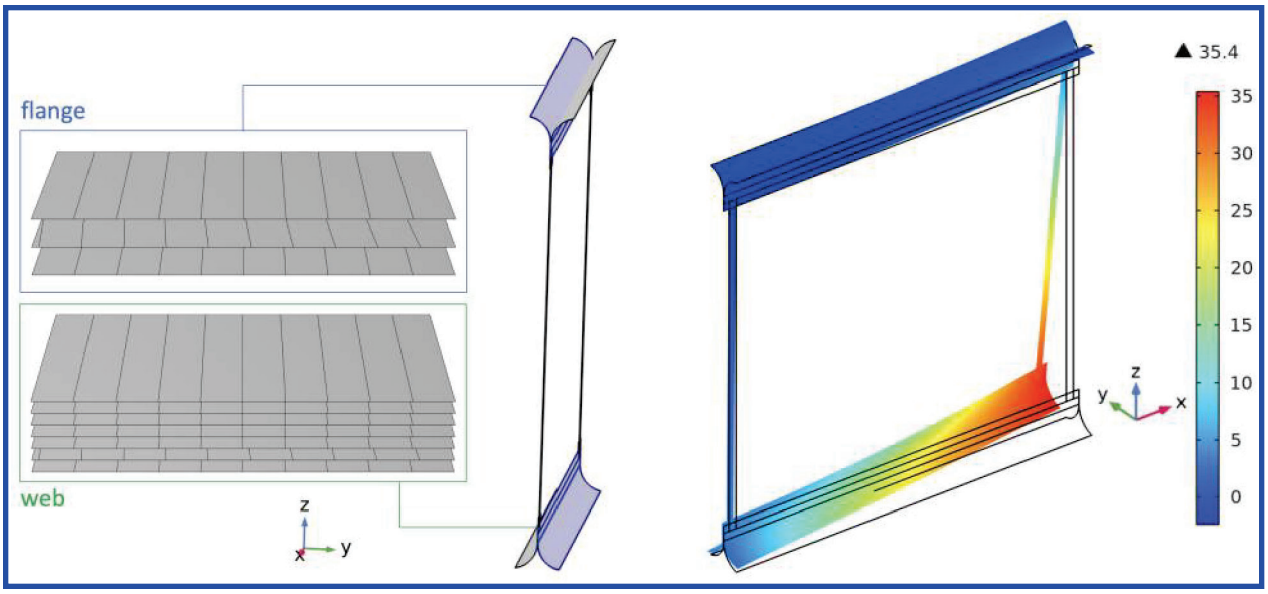

Fig. 7 (left) Location of the two flanges and two webs with (left inset) laminates altered by rotating one of the carbon fiber plies 2°, with (right) the resulting y-displacement field (mm), almost identical to the pristine laminate case above.

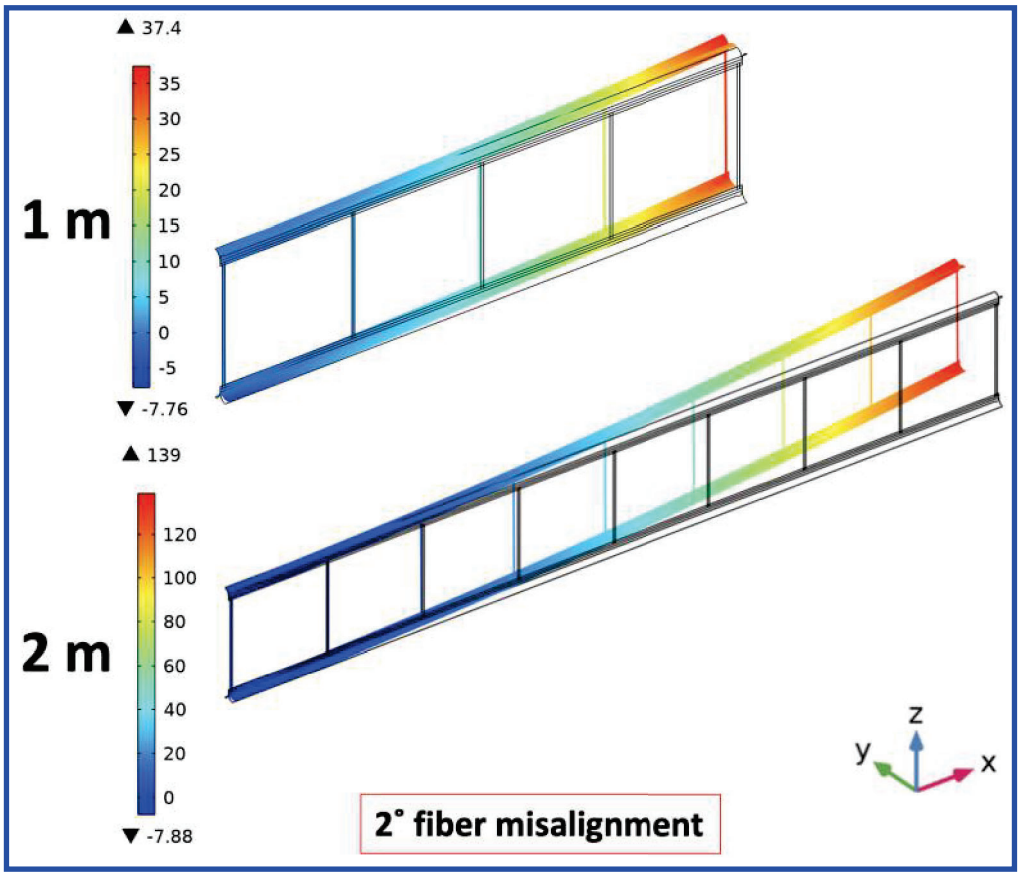

Fig. 8 Deflection (mm) profiles of 1 m and 2 m strips clamped at the upper-right corner with fiber misalignment in the same laminate configuration as the 25 cm case presented above.

is only affected by 12.8 mm, or about 1% of the total deflection.

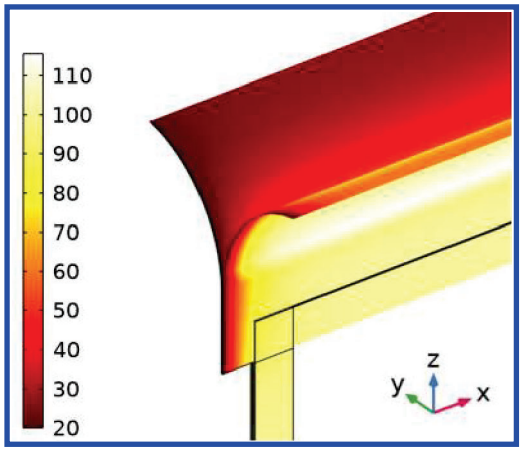

Fig. 9 Detail of the heat-affected zone of the structure at the clamped root when heat is allowed to flow into the root, for a k_1 of 0.99 $\frac{W}{m^2K}$, temperatures in °C. The region of reduced temperature only penetrates a few millimeters into the longeron.

Despite this, k_1 remains an important factor in the deflection of long structures. Under sunlight, when large deflections cause significant variation in local heating angle, the temperature field along the structure will also significantly vary; how well heat travels along the structure between such differently heated regions is entirely a function of k_1. However, if the magnitude of k_1 is small enough, such local variations may be unable to spread enough to make a difference in the overall deflection. Simulations that include the change in heating due to a change in deflection, while attempted in Section III.D, are beyond the scope of the current analysis.

2. Effect of k_2

The conductivity *transverse to* the fiber direction, i.e. *across* the flanges and web of the structure, has a more direct impact on the steady-state temperatures along the length of the structure, regardless of whether heat flows into the root clamp. In turn, since the thermal gradients (and expansions) along the flanges perpendicular to the fiber direction are the dominant cause of deflections therein, we would expect a variation in k_2 to have an enormous impact on the structure's deflection.

For our composite laminates, k_2 is roughly one-fourth of k_1 for the same laminate ($\sim 0.27 \frac{W}{m^2K}$). Upon simulating this value of k_2 for the 5 m structure, when compared with $k_2 = 0.001 \frac{W}{m^2K}$ (i.e. ~ 0) as a baseline value, the temperature field was affected by less than 0.01°C, while the deflection field was affected by a maximum of 1.9 mm. Even the upper bound on experimentally determined k_2, $0.66 \frac{W}{m^2K}$, only affected the maximum deflection by 3.5 mm; in fact, non-negligible effects on these two metrics were not found until the value of k_2 was two orders of magnitude higher, at which point the effects became very significant ($\sim$38% less deflection). However, since our measured values of k_2 are much lower, these results imply that *k_2 for our laminates and structures can be considered to be ~ 0.*

This is an interesting point from the perspective of thin composite thermal property measurement and modeling: the small thermal conductivity across the fibers, despite being the dominant cause of thermal gradients and deflections, can be approximated as 0 with almost no loss of accuracy.

3. Effect of Realistic Initial Twist

A common manufacturing defect in carbon-fiber strip structures is the presence of twist, both in the longerons themselves and in the structure formed by the two longerons; in addition, the lack of out-of-plane torsional stiffness in the basic unit magnifies any existing twist present in the longerons or battens. Unintentional twisting from any of these causes during the manufacturing process manifests itself in the twisting of the entire structure about the longitudinal axis unless twisting is prevented.

The effect is introduced here by modifying the structural geometry such that it forms a helical ladder shape. No residual stresses are induced by such a definition; this matches the negligible stresses that appear to be present in a nearly

perfect sample allowed to twist. Experimentally, a fraction of a sample ultralight structure's self-weight is sufficient to completely straighten it, showing the smallness of the residual internal forces.

The value of the longitudinal twist, chosen to be 4.8° per structural unit, was taken from measurements of the unit tested in Section IV and assumed to add for each structural unit added. Therefore, a four-unit structure would have a twist of 19.2°. Additionally, assuming this twisting chirality to be random, both 4.8° and -4.8° of twist were simulated – positive twist being counterclockwise as viewed looking down the structure to the root, and negative being clockwise.

Results for +4.8° twisting angles are presented in Figure 10, and for -4.8° twisting angles in Figure 11. When compared with the results for untwisted structures under identical heating in Figure 6, the difference is dramatic: even for the smallest structure, less than five degrees of structural twist causes deflections 50% of the magnitude *in the other direction!* This sensitivity indicates how much the temperature field and gradients are affected by structural deflections; even a small change in structural geometry has an outsized effect on the final deflection result.

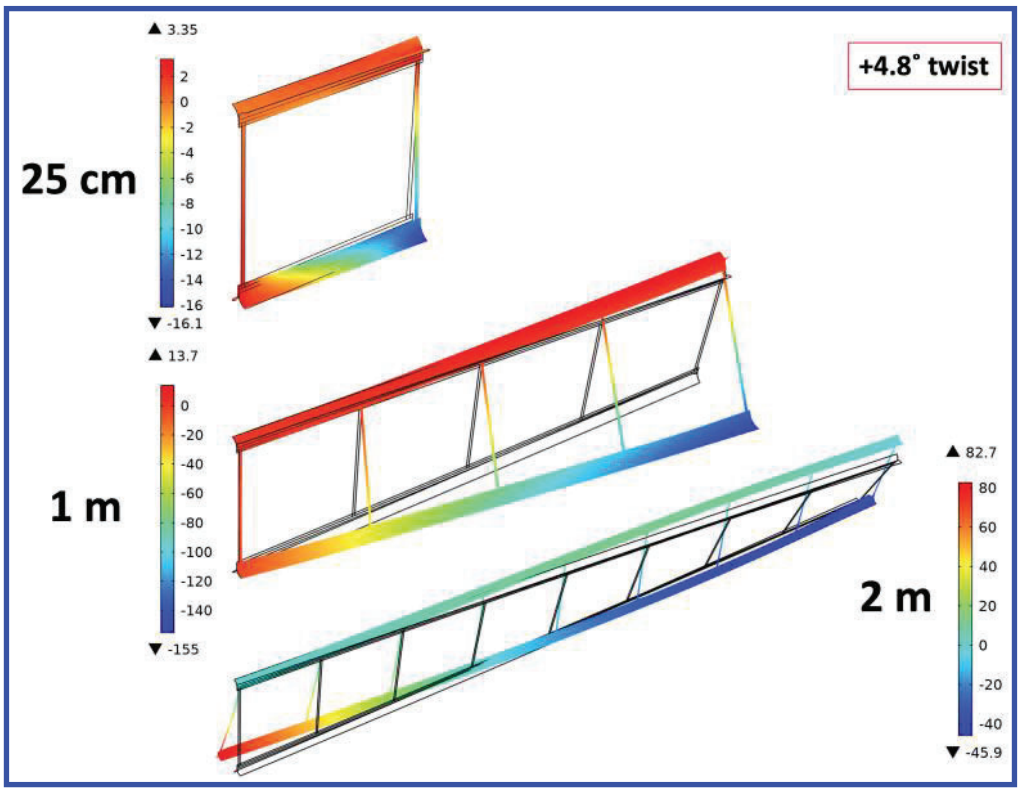

Fig. 10 Deflection (mm) profiles of 25 cm, 1 m, and 2 m strips clamped at the upper-right corner with realistic initial twist, +4.8° (i.e. counterclockwise looking down toward the clamped root).

4. Effect of k_1 with Twist

Since structural twist produces a spatially varying temperature field, one might think the effect of k_1 would become noticeable – but upon examination of both twist angles (±4.8°) for the 25 cm, 1 m, and 2 m models, no difference in deflection greater than 0.1 mm was observed for any case, even for values of k_1 two orders of magnitude higher than that of our material samples.

D. Geometrically Nonlinear Simulations

Finally, stationary, coupled, geometrically *nonlinear* simulations were performed on the untwisted 25 cm, 1 m, and 2 m structural models. In these simulations, the final heating load is achieved by slowly ramping up the heat load, calculating deflections along the way while taking into account any buckling behavior that may occur. Long before the nominal value of the solar flux was reached, however, highly nonlinear buckling effects were encountered for all structure lengths. As the heat flux was ramped from 0 to the nominal solar constant of $1354 \frac{W}{m^2}$, buckling was observed

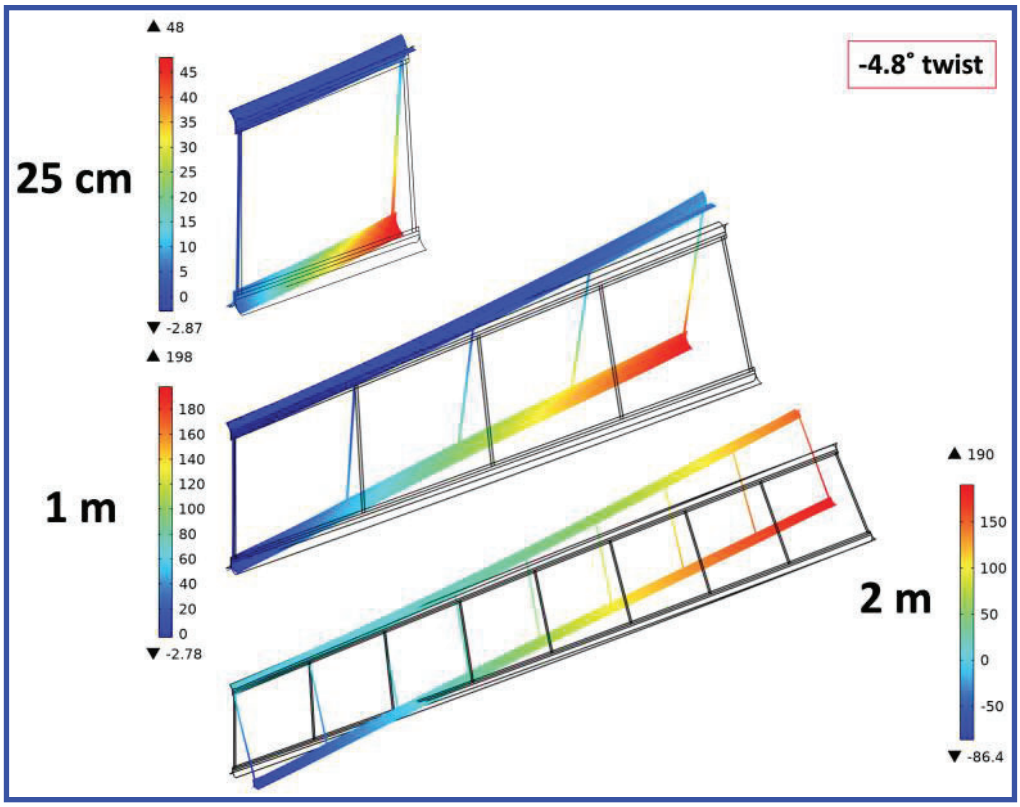

Fig. 11 Deflection (mm) profiles of 25 cm, 1 m, and 2m strips clamped at the upper-right corner with realistic initial twist, -4.8° (i.e. clockwise looking down toward the clamped root).

relatively early on in the ramping process, severely limiting the ability of the solver to approach the final nominal value in later cases. The longer the structure became, the earlier the solver failed to converge in the ramp. Figure 12 shows the nonlinear deflection results at the maximum flux for which each structure was successfully able to converge, while Figure 13 compares the linear and nonlinear deflection predictions for each structure recalculated at this maximum flux.

Unfortunately, COMSOL is unable to recalculate the radiative view factors in any simulation other than a geometrically nonlinear *and time-dependent* analysis; this recalculation is critical to obtaining a radiation and subsequently a temperature field that is different from the small-deflection case. Further, the significant nonlinear buckling behavior of the structures in a steady-state analysis rendered them almost totally unable to be modeled in a transient analysis.

The longest time duration for which a solution converged at the nominal solar heat flux was 0.0039 seconds, and even attempting to update the radiation view factors every 0.0009 seconds failed to reproduce the desired change in local irradiation across the structures. Therefore, for *untwisted* structures, obtaining deflection results that truly couple to the radiative field varying along the length, which in turn results in a temperature field varying along the length, still proves elusive, and would appear to be best pursued with other software such as Abaqus or Thermal Desktop.

IV. Experimental Verification in Vacuum

To verify the results of the 25 cm structure, an experimental setup has been constructed. A 25 cm strip sample was manufactured, suspended from an aluminum frame, and heated by a quartz infrared heater (QIH) lamp; this lamp is surrounded by a double reflector to collimate its light into a uniform flux at the distance of the structure. The strip is instrumented with thin lightweight thermocouples to directly measure temperature on the front and back flanges, while two cameras measure the in- and out-of-plane deflections via Digital Image Correlation (DIC). The entire setup (excluding the cameras) is situated inside an acrylic vacuum chamber, capable of greatly reducing convection by dropping the ambient pressure to around 5% atmospheric pressure. The setup is presented in Figure 14.

To collimate the rays of the heat lamp, the double reflector shown in Figure 15 was constructed. The heat lamp is mounted at the focus; rays of light going backwards from the lamp hit the parabolic reflector and are reflected forward,

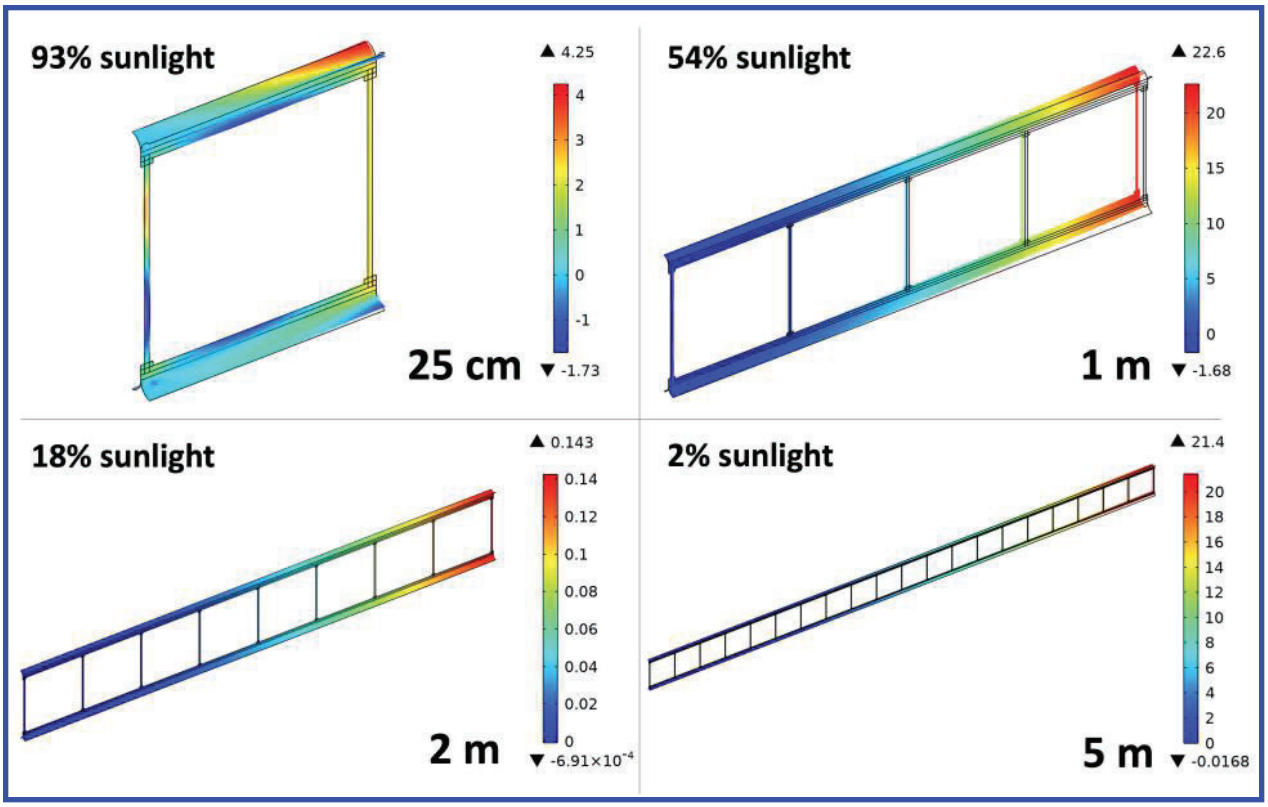

Fig. 12 Deflection (mm) profiles of 25 cm, 1 m, 2 m, and 5 m strips clamped at the upper-right corner with geometric *nonlinearity* simulated, each at the maximum heat flux that successfully converged. Buckles have formed in a few battens – note the leftmost batten of the 25 cm structure.

while rays going forward hit the inside of the cylindrical reflector and are reflected backwards. The net result, as verified by a ray-tracing simulation, is a well-collimated beam of light impinging on the strip structure, with heat flux varying less than 5% over the strip. There is a dead zone of low radiation directly in front of the cylindrical reflector, but it is partially washed out by edge effects at a distance of 30 cm, which is where the test structure has been placed. Furthermore, only a small section of the two battens is affected by this dead zone – neither of which contribute very much to the deflection response, in comparison to the longerons.

To reduce the heat load on the chamber produced by the ~100 W lamp, two means of removing heat from the chamber are employed: 1) chilling the baseplate through the chamber underside using a water chiller and coolant loop, and 2) cooling a 0.5" steel plate in a -30° freezer for several hours, then placing it into the chamber directly behind the unit structure. Together, these heat sinks are able to keep the chamber walls at much lower temperatures, as well as produce a sufficiently large thermal gradient on the structure.

To obtain detailed displacement measurements before, during, and after heating, Digital Image Correlation (DIC) was used: two digital cameras mounted in stereoscopic configuration were positioned outside the vacuum chamber.

Two large LED lights illuminated the sample. To minimize DIC analysis errors caused by nonuniform illumination, shadowing of the strip, and glinting reflections, the lights were carefully positioned such that their light entered from the top of the chamber and bounced off a reflective aluminum foil panel onto the top and bottom flanges. The resulting light was sufficiently diffuse across both strips, but was visibly dimmer on the top flange.

Calibration of this test setup, as detailed in [4], was a nontrivial task due to the large refractive effects caused by the thick walls of the acrylic vacuum chamber, amplified by their further bowing inwards while supporting a vacuum. The corrective procedure involved three main steps: 1) calibrating the setup with a rigid grid and applying a variable ray origin (VRO) calibration, 2) taking DIC images without vacuum to extract the baseline deflection, 3) taking DIC images under vacuum during the experiment, and 4) subtracting the results of step 2) from step 3) to obtain the final deflection measurements.

The main deflection results will be presented in an upcoming publication, but a representative snapshot of the real

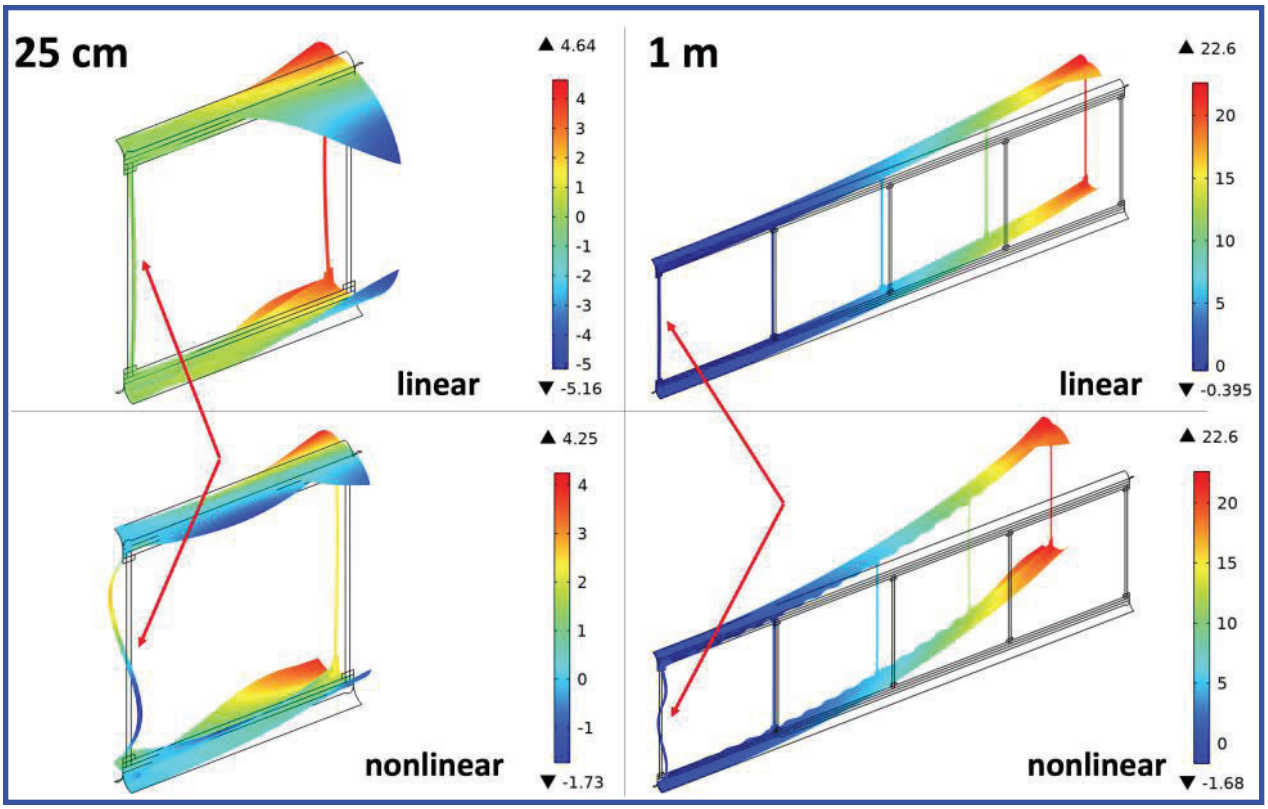

Fig. 13 Exaggerated deflection (mm) profiles of 25 cm and 1 m strips with geometrically linear and nonlinear simulations compared, each at the maximum heat flux that successfully converged (deflection exaggerated by a factor of 10). Note the nonlinear buckles on the leftmost battens.

structural unit's deflection behavior is shown in Figure 16, along with extracted data from the top and bottom flanges in Figure 17. Under a radiative heat load of around 40% of the solar constant (i.e. ~500 $\frac{W}{m^2}$) and different radiative surroundings, the structure achieves maximum out-of-plane deflections between 0.1-0.4 mm on the top flange and between 0.25-1 mm on the bottom flange. These deflections are smaller than the deflections presented in this work, due to both the smaller lamp flux and very different radiative boundary conditions: the chamber walls, cooled plate, and cooled baseplate do not behave the same as the uniform radiative backdrop condition used in this work's simulations. In addition, non-negligible convection in the near-vacuum environment dilutes the thermal gradients and therefore reduces deflections further. In fact, the experimental deflections are actually several times *larger* than current simulations of the entire chamber predict for this geometry. Even so, these results show that non-negligible deformations do in fact occur in thin composite structures, and are thus worthy of further simulation and study.

V. Conclusions and Future Work

The temperature and deflection profiles simulated thus far show that, with real-life values of composite laminate thermal properties, large scale deflections occur at any significant length of the strip architecture studied. Such large temperature gradients have been simulated in other works [1], but the lower assumed thermal expansion coefficients of the simulated composites meant that large deflections were not predicted. Direct thermal property measurements for the strip laminates were an order of magnitude higher than these assumed values, leading too much greater deflections than previous predictions. This cause-and-effect was and will be bolstered by further experimental evidence.

Several factors affecting the temperature and deflection fields were examined for these structures, including laminar fiber misalignment, in-plane thermal conductivity, and residual twisting. All except the last were shown to have virtually no effect on simulated deflections, owing to the high strength and very low thermal conductivity of the composite laminates used. Residual twisting, however, was shown to significantly impact structural deflection, with only a few degrees of twist needed to *completely reverse* the direction of predicted deflection. The mechanism for this sensitivity is

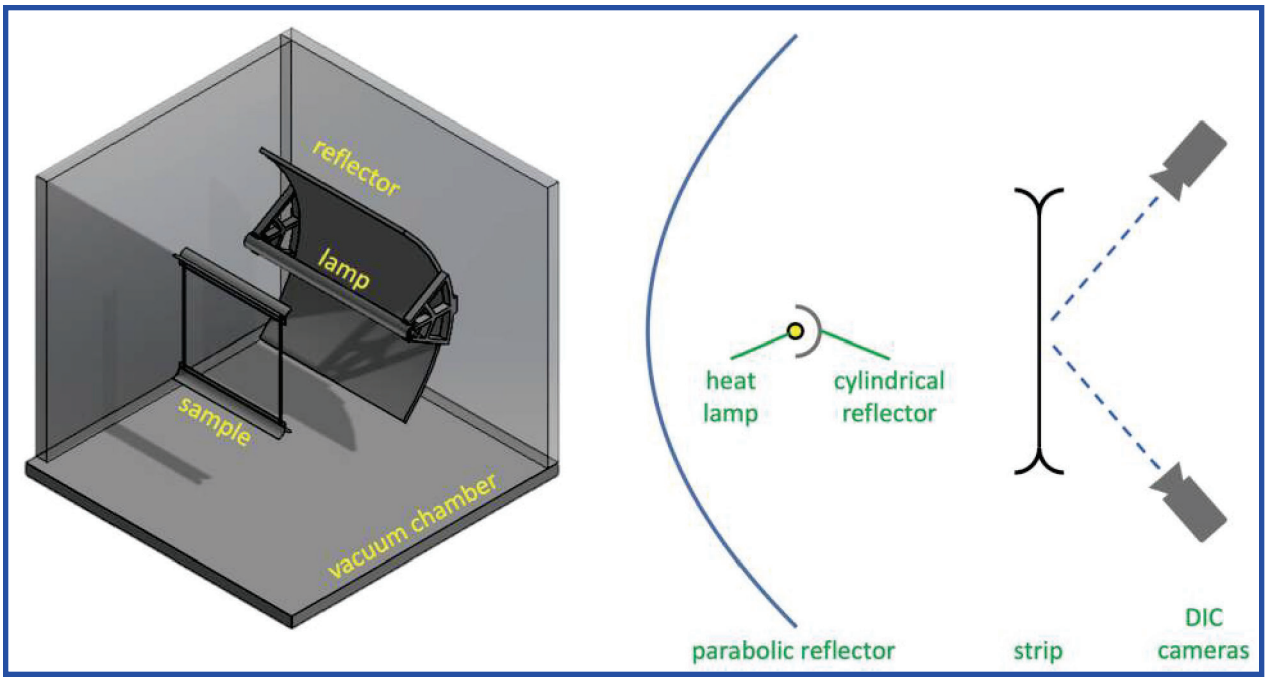

Fig. 14 (left) An isometric drawing showing the main components of the experiment, with (right) a side view showing the main components.

presumed to be the effect of twisting on local radiant heating angle, which leads to non-uniform temperature fields across the structure and thus to varying thermal gradients and deflections.

In addition, these simulations offer a unique insight into the thermal deflections of realistic space structures made of realistic materials, taking into account current construction techniques and even various manufacturing defects. Such imperfections are commonly known – and have been demonstrated in the present study – to have a large impact on thin shell structures, offering more accurate insight into the behavior of current and future space structures.

Acknowledgments

The authors would like to acknowledge Eric Sunada, Thermal Technologist in Propulsion, Thermal, and Materials Systems at the Jet Propulsion Laboratory, for his insight on thermal experiments, modeling, and material support. The National Science Foundation's Graduate Research Fellowship Program, as well as the Caltech Space Solar Power Project, provided financial support for this research.

References

[1] Stohlman, O. R., and Loper, E., "Thermal deformation of very slender TRAC booms," *3rd AIAA Spacecraft Structures Conference*, 2016. https://doi.org/10.2514/6.2016-1469.

[2] Stohlman, O. R., "Coupled radiative thermal and nonlinear stress analysis for thermal deformation in large space structures," *5th AIAA Spacecraft Structures Conference*, 2018. https://doi.org/10.2514/6.2018-0448.

[3] Thornton, E. A., *Thermal Structures for Aerospace Applications*, 1st ed., American Institute of Aeronautics and Astronautics, 1996, Chaps. 4, 9.

[4] Pederson, J., Haraszti, A., and Pellegrino, S., "Thermoelastic Deformations of Thin-Shell Deployable Booms," *AIAA SCITECH 2023 Forum*, 2023. https://doi.org/10.7907/X60S-BR30.

[5] Blandino, J. R., "Analysis of thermal-mechanical interactions of STEM booms," *2nd AIAA Spacecraft Structures Conference*, 2015. https://doi.org/10.2514/6.2015-1164.

[6] Chamberlain, M. K., Kiefer, S. H., and Banik, J., "On-orbit structural dynamics performance of the roll-out solar array," *5th AIAA Spacecraft Structures Conference*, 2018. https://doi.org/10.2514/6.2018-1942.

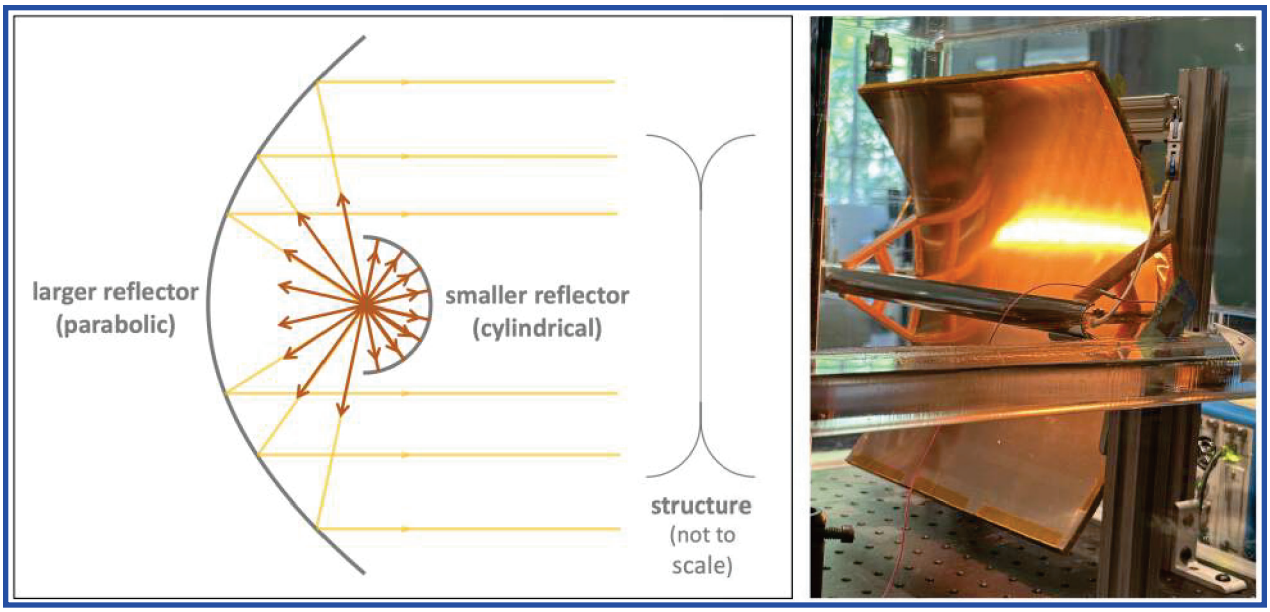

Fig. 15 (left) A 2D ray diagram of the two-part heat lamp reflector apparatus along its focal axis, illustrating how the lamp's point source rays are reflected into a collimated beam. The smaller cylindrical reflector reflects forward-going lamp rays back towards the larger parabolic reflector. (right) The reflector apparatus as-built, mounted in the acrylic vacuum chamber; one of the chamber's reinforcement ribs lies in the foreground. Note the diffused reflection of the lamp in the larger reflector.

[7] Mahaney, J., and Thornton, E. A., "Self-Shadowing Effects on the Thermal-Structural Response of Orbiting Trusses," *Journal of Spacecraft and Rockets*, Vol. 24, No. 4, 1987, pp. 342–348. https://doi.org/10.2514/3.25922.

[8] Gdoutos, E. E., Sommer, C. F., Truong, A., Wen, A., Pedivellano, A., Ubamanyu, U. K., Madonna, R. G., and Pellegrino, S., "Development of the Deployable on-Orbit ultraLight Composite Experiment (DOLCE) for the Space Solar Power Project (SSPP) Demonstration Mission," *AIAA SCITECH 2022 Forum*, 2022, p. 1266. https://doi.org/10.2514/6.2022-1266.

[9] The Composites Store, C. S. T., "Comparison Data for Pultruded Shapes," , 2018. URL https://www.cstsales.com/rod_comp.html.

[10] Leclerc, C., "Mechanics of Ultra-Thin Composite Coilable Structures," Dissertation (Ph.D.), California Institute of Technology, 2020. https://doi.org/10.7907/X60S-BR30.

[11] Ubamanyu, U. K., "Time-dependent Failure of Thin-ply Composite Laminates," Dissertation (Ph.D.), California Institute of Technology, 2023. https://doi.org/10.2514/6.2022-1266.

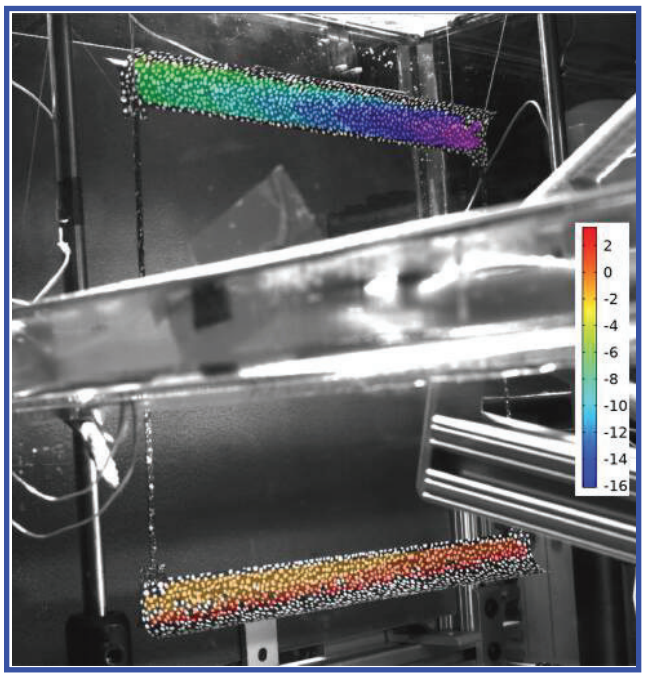

Fig. 16 A snapshot of the full-field out-of-plane deflection (μm) data extracted during the Digital Image Correlation process.

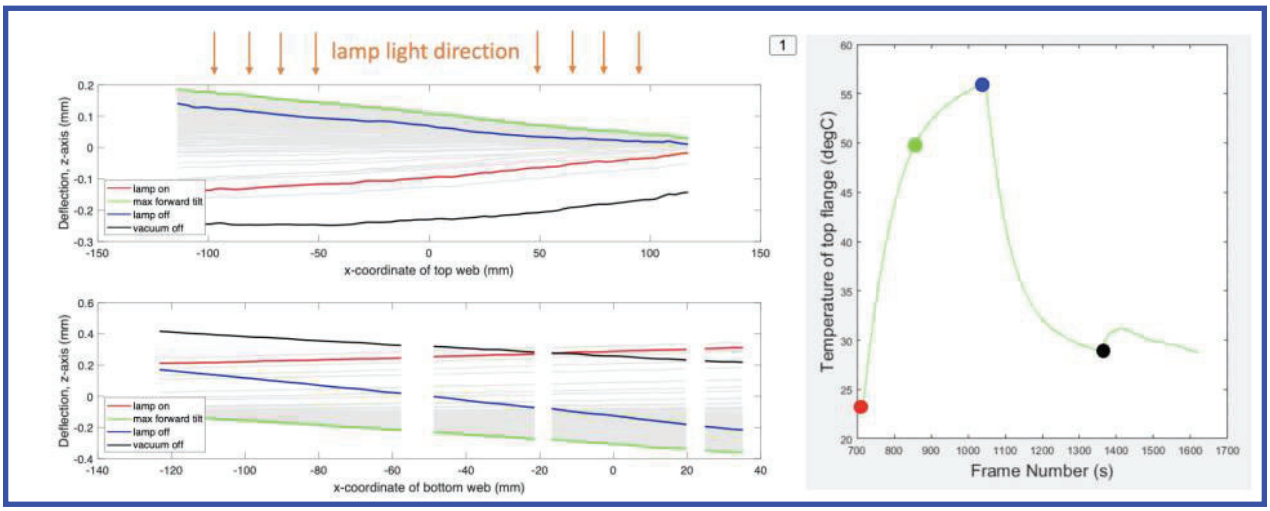

Fig. 17 (left) The deflection of the top and bottom flanges at four snapshots in time, specified on the (right) green temperature curve of the flange thermocouple data. From a baseline (red) defined to be zero at time $t = 0$, the structure tilts forward (green) such that the top flange moves toward the lamp and the bottom moves away, then tilts away from the lamp (blue) before the lamp is turned off and tilts even further away (black).